Growth induced magnetic and chemical anisotropy in $CoPt_3$ alloy films

J. O. Cross,[a]* M. Newville,[b] F. Hellman,[c] P. W. Rooney,[c] A. L. Shapiro[c] and V. G. Harris[d]

[a]PNC-CAT, Advanced Photon Source, Argonne National Laboratory, Argonne, IL 60439 U.S.A., [b]University of Chicago, 5640 S. Ellis Avenue, Chicago, IL 60637, [c]Department of Physics, University of California at San Diego, La Jolla, CA 92093, and [d]Complex Materials Section, Code 6342, Naval Research Laboratory, Washington, DC 20375-5000. E-mail: jox@pnc.aps.anl.gov

We report the results of polarized Co *K* EXAFS experiments on a series of $CoPt_3$ films grown by molecular beam epitaxy on (100) MgO single crystal substrates over a range of temperatures from 473 K to 1073 K. These samples exhibit substantial perpendicular magnetic anisotropy that is strongly dependent on the substrate growth temperature T_g. We measure a preference for in-plane Co-Co pairs that is correlated with the magnetic properties.

1. Introduction

Materials for magneto-optic (MO) storage applications require Curie temperatures (T_C) greater than room temperature, but low enough for diode laser writing via localized heating above T_C; a large Kerr rotation, for robust read signals; large coercivity, to protect the written bit against accidental erasure; and, preferably, a perpendicular magnetic anisotropy (PMA) to provide the media with an intrinsic high-density storage capability.

Presently, the predominant MO materials for storage applications are amorphous rare earth-transition metal (α-RETM) alloys, *e.g.*, TbGdFeCo. Co/Pt multilayers, which have a pronounced magneto-optic response to blue light, have been suggested as alternatives for the next generation of MO materials (Lin & Gorman, 1992; Weller, 1992), however multilayer growth remains prohibitively complex for large scale commercial processing.

Recently, Co_xPt_{1-x} alloy films, $x \approx 0.25$, have been prepared that exhibit PMA comparable to that of Co/Pt multilayers and T_C as high as 673 K (Rooney *et al.*, 1995). This is in stark contrast to the equivalent bulk alloys which are nonmagnetic and have a T_C of 483 K.

Several researchers were quick to suggest that some form of Co segregation must be present in the alloy films to account for the PMA and high T_C. However, careful TEM and XRD (Shapiro *et al.*, 1999) studies show these films to be of high crystalline quality, with the same long range order as the bulk alloys, i.e., Cu_3Au structure when they are grown above $T_g > 903$ K, or chemically disordered fcc for $T_g < 903$ K.

One early XAFS study (Tyson *et al.*, 1996) on a single (111) alloy film in the peak PMA regime $Co_{0.28}Pt_{0.72}$ found an excess of in-plane Co-Co bonds. A more recent and rigorous XAFS study (Meneghini *et al.*, 1999) of $CoPt_3$ (111) and Co_3Pt (0001) films found that both systems show growth induced chemical anisotropy in the minority component, and that the Co-Co pair anisotropy is correlated with the appearance of PMA. A similar correlation between magnetic and chemical anisotropy was seen in earlier studies on α-TbFe films, and found to be responsible for the PMA in that system (Harris *et al.*, 1994). Studies of the magnetic behavior of films grown by molecular beam epitaxy have found growth induced magnetic anisotropy in (100), (111) and (110) oriented films, and the effect seems to be independent of film thickness (Shapiro *et al.*, 1999).

In this report, we present the results of polarized Co *K* EXAFS on a series of (100) $CoPt_3$ films grown by molecular beam epitaxy on (100) MgO single crystal substrates over a range of temperatures from 473 K to 1073 K. The films were approximately 2000Å thick. The bulk structural and magnetic properties of these samples have been well characterized and reported elsewhere (Shapiro *et al.*, 1999). The net magnetic anisotropy K_μ is measured to increase with T_g from near zero at 473 K to 6.5×10^6 erg/cc at 673 K before it diminishes to a value near zero at $T_g \sim 823$ K. The Curie temperature closely tracks this effect, peaking at a value of 693 K for T_g of 673 K and approaching the value of the bulk disordered alloy for growth temperatures less than 473 K and greater than 823 K. We find a T_g dependent preference for in-plane Co-Co bonds that is correlated with K_μ.

2. Experimental

The EXAFS measurements were performed at the Advanced Photon Source, using the PNC-CAT undulator beamline 20-ID-B. Properties of the beamline are reported elsewhere in these proceedings (Heald *et al.*, 2000). A fixed-exit cryogenically cooled Si (111) monochromator was used to select the incident x-ray energy across the Co *K* and Pt L_{III} absorption edges, using the first and third harmonics of the undulator, respectively. The Pt data will be reported elsewhere. The undulator gap was scanned with the monochromator to maintain the peak of the harmonic.

The samples were mounted on a 6000 rpm spinner to minimize the effect of Bragg diffraction from the MgO substrate and the fcc $CoPt_3$ film. Sample and spinner were mounted on a variable tilt stage set at $5^\circ \pm 1^\circ$ to the unfocused incident beam. tantalum slits were used to define the beam. Typical slit sizes to underfill the samples were around 0.1–0.2 mm in the glancing angle direction 1.0 mm in the other direction. The slit spacing and sample position were adjusted using a light dusting of ZnS phosphor powder on the sample surface and spinning the sample in the x-ray beam. The visible fluorescence from the phosphor was observed using a CCD camera, and the sample position and slit sizes were adjusted from the control station to optimize the footprint of the beam. After alignment, the phosphor dust was removed using cotton swabs soaked in methanol swiped gently across the spinning surface.

The Co and Pt fluorescence was collected using a sealed gas ionization chamber filled with Ar placed normal to the incident beam direction and in the plane of polarization. The incident beam intensity was monitored using a 300 mm transmission gas ionization chamber with 10 mm plate separation operated at 700 VDC flowing He. Harmonic rejection was accomplished by detuning the second crystal of the monochromator to 35% of peak intensity and locking on this detuning using a PID feedback circuit. Four samples, grown at $T_g = 473$ K, 723 K, 873 K and 1073 K, were measured with the polarization in-plane and out-of-plane of the substrate at the Co *K* and Pt L_{III} absorption edges. Five scans at three seconds/point were collected at each condition.

3. Analysis

The EXAFS analysis was performed following recommendations of the International XAFS Society (Lytle *et al.*, 1989). The pre-edge and background were subtracted from the normalized I_f data sets

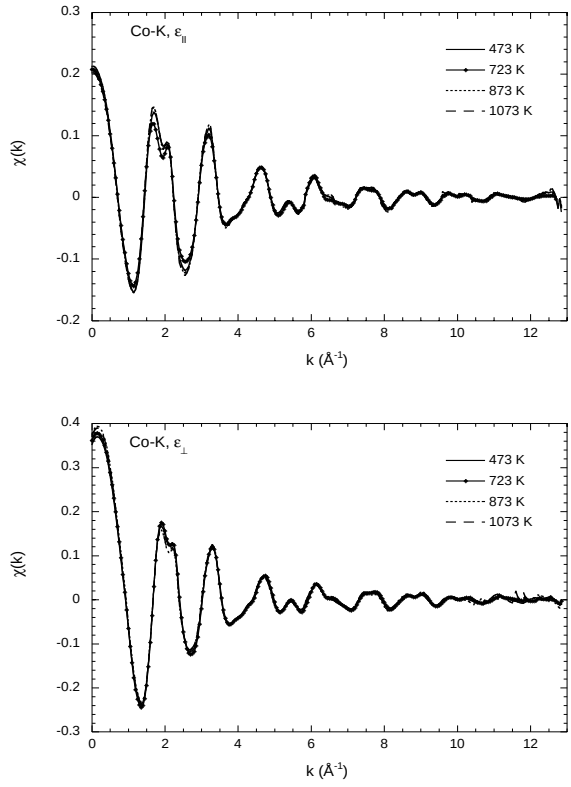

Figure 1
Raw $\chi(k)$ data for $\hat{\epsilon}_\perp$ (upper) and $\hat{\epsilon}_\perp$ (lower). Four substrate temperatures are overplotted in each graph.

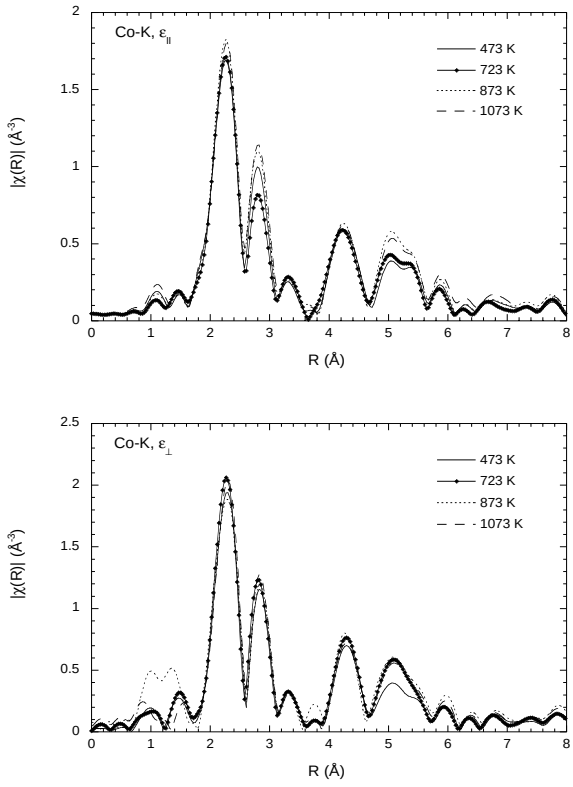

Figure 2
R-space Fourier transforms of the Co *K* EXAFS for $\hat{\epsilon}_\perp$ (upper) and $\hat{\epsilon}_\perp$ (lower). Four substrate temperatures are overplotted in each graph.

using AUTOBK (Newville *et al.*, 1993), and the resulting $\chi(k)$ were averaged before further analysis. Figure 1 shows the $\chi(k)$ for $\hat{\epsilon}_\perp$ and $\hat{\epsilon}_\parallel$ Figure 2 shows the *R*-space Fourier transforms of the Co *K*-edge XAFS data. The transforms were taken between $k = 1.0$ Å^{-1} and $k = 10.5$ Å^{-1} with k^2-weighting and a Hanning window with 0.2 Å^{-1} sills. The *R*-space fits were performed over the first shell between $R = 1.7$ Å and $R = 3.1$ Å, with no phase correction.

The first shell was modeled as a weighted sum of Co-Co and Co-Pt single scattering paths, assuming an average fcc structure, as determined by x-ray diffraction (XRD). Two occupancy parameters α and β were used to describe the amount of Co in the nearest neighbor in-plane and out-of-plane positions, respectively. For a random distribution of Co and Pt, $\alpha = \beta = 0.25$. For the ordered Cu_3Au ($L1_2$) phase, $\alpha = \beta = 0.0$.

For each sample, $\chi(R)$ data for $\hat{\epsilon}_\parallel$ and $\hat{\epsilon}_\perp$ were fit simultaneously subject to self-consistency in the variable path parameters listed in Table 1. The XAFS $\cos^2$ polarization factors were included explicitly[1] in the CoCo and CoPt path amplitudes. Using this model, the contributions to $\chi_{\rm total}$ from the Co and Pt neighbors for the two polarizations are given by

$$\chi_\parallel = 3[\frac{1}{2}\mathrm{N}_\parallel(\alpha\chi_{\rm Co} + (1-\alpha)\chi_{\rm Pt}) + \frac{1}{4}\mathrm{N}_\perp(\beta\chi_{\rm Co} + (1-\beta)\chi_{\rm Pt})] \quad (1)$$

$$\chi_\perp = 3[\frac{1}{2}\mathrm{N}_{\rm out}(\beta\chi_{\rm Co} + (1-\beta)\chi_{\rm Pt})] \quad (2)$$

where $\mathrm{N}_{\rm out} = 8$ and $\mathrm{N}_{\rm in} = 4$ in the ideal fcc lattice. Theoretical phases and amplitudes were calculated using FEFF7 (Ankudinov & Rehr, 1997), and the data were fit in *R*-space using FEFFIT (Newville *et al.*, 1995). The overall amplitude S_0^2 was held fixed at 0.75, determined using the 873 K sample as a reference. A total of eight variable parameters were used to fit the combined $\chi_\perp$ and $\chi_\parallel$ data sets.

The results of the first-shell fit to the 723 K sample for both in-plane and out-of-plane polarization at the Co *K*-edge are given in Table 1, and a graph of the *R*-space data and fit is shown in Figure 3. The individual contributions from the Co and Pt single scattering paths are shown multiplied by -1 on the same graph. Note that the Ramsauer-Townsend resonance in the Pt shell effectively eliminates correlation between CoCo and CoPt paths in the fit, giving a high degree of confidence in the measured anisotropy.

Table 1
Fit results for the first coordination shell in the Co *K*-edge XAFS.

	T_g			
	473 K	723 K	873 K	1073 K
Chemical anisotropy				
α	0.19 ±0.11	0.48 ±0.10	0.12 ±0.09	0.19 ±0.10
β	0.17 ±0.05	0.12 ±0.03	0.11 ±0.06	0.17 ±0.04
Path parameters				
$N_\parallel$	3.63 ±0.19	3.35 ±0.20	3.69 ±0.21	3.58 ±0.17
$N_\perp$	7.84 ±0.23	7.87 ±0.33	7.44 ±0.44	7.59 ±0.18
σ^2_{Co}	0.012±0.004	0.009±0.002	0.007±0.006	0.013±0.003
σ^2_{Pt}	0.007±0.001	0.007±0.001	0.007±0.001	0.006±0.001
R_{Co}	2.664±0.008	2.671±0.008	2.652±0.018	2.663±0.006
R_{Pt}	2.706±0.002	2.691±0.004	2.714±0.006	2.712±0.001

[1] FEFF calculation was performed for isotropic cubic sample and unpolarized x-rays. Polarization dependence of the XAFS from individual scattering paths was written explicitly into the FEFFIT model using a nodegen flag to turn off implicit accounting of path degeneracies.

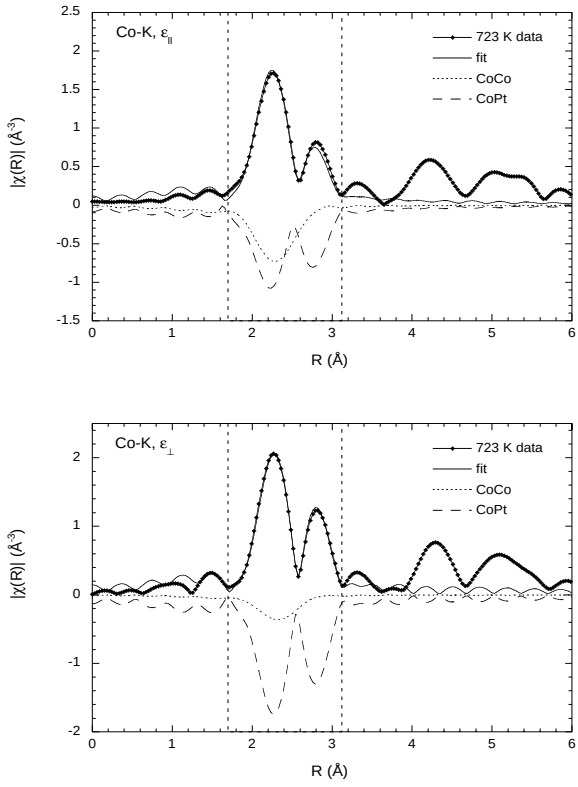

Figure 3
First shell fit to in-plane and out-of-plane polarized XAFS for the $T_g = 723$ K film. The contributions from Pt and Co first neighbors, multiplied by -1 are also shown. This were performed on both data sets simultaneously, subject to self-consistency in the variable path parameters.

4. Conclusion

The distribution of Co-Co pairs in (100) $CoPt_3$ alloy films grown epitaxially on MgO has been measured as a function of T_g. We find that the chemical anisotropy is correlated with the magnetic anisotropy K_μ. Tyson *et al.* (Tyson *et al.*, 1996), have suggested the possibility of anisotropic "plates" or one-dimensional "chains" of Co atoms. Our findings are not inconsistent with this for the film grown at 723 K, however, our measurements can not distinguish these two geometries. Due to the lack of any significant increase in the number of Co-Co bonds out-of-plane, the EXAFS gives an estimate of the out-of-plane extent of the domains as one monolayer.

We note that some anisotropy is evident in the fourth shell for the 723 K sample. In the fcc structure, the fourth shell XAFS signal is dominated by contributions from multiple-scattering paths that focus through the cube face atoms. Exploratory FEFF simulations indicate that the observed anisotropy in this shell may be fully accounted for by the anisotropy in the focusing atoms found in the first shell. Further analysis using regularization methods is planned.

Acknowledgements

The experiments were carried out at sector 20-ID of the Advanced Photon Source. Use of the Advanced Photon Source was supported by the U.S. Department of Energy, Basic Energy Sciences, Office of Science, under Contract No. W-31-109-Eng-38.

References

Ankudinov, A. L. & Rehr, J. J. (1997). *Phys. Rev. B* **56**, R1712–R1715.

Harris, V. G., Elam, W. T., Koon, N. C. & Hellman, F. (1994). *Phys. Rev. B* **49**, R3637–3640.

Heald, S., Stern, E., Brewe, D., Jiang, D., Gordon, R., Crozier, D. & Cross, J. (2000). *J. Synch. Rad., these proceedings*.

Lin & Gorman (1992). *Appl. Phys. Lett.* **61**, 1600–1602.

Lytle, F. W., Sayers, D. E. & Stern, E. A. (1989). *Physica B* **158**, 701–722.

Meneghini, C., Maret, M., Parasote, V., Cadeville, M. C., Hazemann, J. L., Cortex, R. & Colonna, S. (1999). *Eur. Phys. J. B* **7**, 347–357.

Newville, M., P. Līviņš, Yacoby, Y., Rehr, J. J. & Stern, E. A. (1993). *Phys. Rev. B* **47**(21), 14126–14131.

Newville, M., Ravel, B., Haskel, D., Rehr, J. J., Stern, E. A. & Yacoby, Y. (1995). *Physica B* **208&209**, 154–156.

Rooney, P. W., Shapiro, A. L., Tran, M. Q. & Hellman, F. (1995). *Phys. Rev. Lett.* **75**, 1843–1846.

Shapiro, A. L., Rooney, P. W., Tran, M. Q., Hellman, F., Ring, K. M., Kavanagh, K. L., Rellinghaus, B. & Weller, D. (1999). *Phys. Rev. B* **60**, 12826–12836.

Tyson, T. A., Conradson, S. D., Farrow, R. F. C. & Jones, B. A. (1996). *Phys. Rev. B* **54**, R3702–R3705.

Weller, D., Brändle, H., Gorman, G., Lin, C. J, & Notarys, H. (1992). *Appl. Phys. Lett.* **61**, 2726-2728.